



ARTICLE

## Fabrication of High Toughness Silk Fibroin/Tungsten Disulfide Nanoparticles Hybrid Fiber and Self-Heating Textile by Wet Spinning

Jianjun Guo<sup>1,2</sup>, Lingling Jia<sup>3</sup>, Sandra Senyo Fometu<sup>4</sup>, Qiang Ma<sup>5</sup>, Jinjin Wang<sup>1</sup>, Hang Li<sup>1</sup>, Lei Jiang<sup>5</sup> and Guohua Wu<sup>1,\*</sup>

<sup>1</sup>College of Biotechnology, Jiangsu University of Science and Technology, Zhenjiang, 212100, China

<sup>2</sup>College of Agriculture, Anshun University, Anshun, 561000, China

<sup>3</sup>College of Food and Pharmaceutical Sciences, Ningbo University, Ningbo, 315800, China

<sup>4</sup>Biofuels Institute, School of Environment and Safety Engineering, Jiangsu University, Zhenjiang, 212013, China

<sup>5</sup>College of Environmental and Chemical Engineering, Jiangsu University of Science and Technology, Zhenjiang, 212100, China

\*Corresponding Author: Guohua Wu. Email: ghwu@just.edu.cn

Received: 27 December 2021 Accepted: 27 January 2022

### ABSTRACT

Traditionally, silkworm silk has been used to make high-quality textiles. Nevertheless, various wastes from silkworm silk textiles that are no longer used are increasing, which is also causing considerable waste and contamination. This issue is causing widespread concern in countries that use more silk. Regenerated silk fibroin (RSF) fibers have been shown to be fragile and tender, which prohibits RSF from being widely used as a structural component. Therefore, enriching the function of silk and enhancing the RSF mechanical properties are important directions to expand the comprehensive utilization of silk products. In the present research, wet spinning was used to create a series of RSF/tungsten disulfide (WS<sub>2</sub>) nanoparticles (NPs) hybrid fiber having distinct WS<sub>2</sub> nanoparticles concentrations. It was discovered that the temperature of hybrid fibers containing 0.8 wt% RSF/WS<sub>2</sub> nanoparticles might climb from 20.4°C to 85.6°C in 1 min and 108.3°C in 10 min after being exposed to simulated sunlight for a period of one minute and ten minutes. It also had certain antibacterial activity and thermal stability. Fabrics created by hand mixing had outstanding photothermal characteristics under natural sunlight. Furthermore, adding WS<sub>2</sub> nanoparticles might increase the tensile properties of hybrid fibers, which could be caused by the reality that the blending of WS<sub>2</sub> nanoparticles inhibited the self-assembly of β-sheets in RSF reaction mixture in a dosage-dependent way, as evidenced by the fact that RSF/WS<sub>2</sub> nanoparticles hybrid fibers had lesser β-sheets material, crystalline nature, and crystalline size. The above performance makes the RSF/WS<sub>2</sub> nanoparticles hybrid fibers promising candidates for application in photothermal fabrics as well as military clothing.

### KEYWORDS

Smart textile; wet spinning; high toughness; photothermal conversion; regenerated silk fibroin

## 1 Introduction

The textile industry has evolved into one of the biggest and the most traditional sectors in the world, with a market valuation estimated to be over USD 1.3 trillion and provides job possibilities for more than 300 million individuals throughout the chain of production [1]. Nevertheless, fast fashion in the textile



This work is licensed under a Creative Commons Attribution 4.0 International License, which permits unrestricted use, distribution, and reproduction in any medium, provided the original work is properly cited.

field has caused numerous waste textile, resulting in serious problems such as resource shortage and environmental pollution [2]. For instance, the recycling and recovery business in the United States reports that it recycles roughly 3.8 billion pounds of post-consumer textile waste annually (15 percent). However, 85 percent of the waste is treated with landfills [3]. In 2019, 720,800 tons of cocoons and 68,600 tons of raw silk were produced in China, accounting for more than 80% of the world. Most of them were used in the textile industry, although only a small percent of about one percent of textile waste is recycled and reused [3]. The recycling and reuse of massive waste textiles need to be strengthened urgently.

Silk fibroin is the primary constituent of silk fibers, and it may be recovered and reutilized by solubilizing old silk materials. A growing body of research evidence has demonstrated that comparable to natural silk, regenerated silk fibroin (RSF) possesses non-toxic, non-allergic, and excellent biodegradability and biocompatibility [4,5]. In waste silk products, there is still substantial potential value that can be recycled. A large number of researchers are focused on increasing the holistic utilization of disposed silk products by enhancing their functional properties using RSF fibers [6,7]. Wet spinning is among the technologies that may be used to manufacture RSF fibers with a variety of morphological features and properties. Nonetheless, the structural properties of RSF fibers generated through wet spinning are frequently poorer than those of natural silk, which has severely restricted its application ranges [8,9]. As a result, more research is required to optimize the physical properties of these fibers.

Photothermal materials have been shown to possess exceptional optical-thermal properties and have the potential to be used in a variety of applications, including the production of textiles, medical devices, novel drug carriers, and the manufacture of military-type gear [10,11]. Researchers have been exploring ways to incorporate photothermal elements into polymer fibers, thus producing improved photothermal textiles to ensure the quality of textile fabrics [12–14]. Tungsten disulfide (WS<sub>2</sub>) has good light-to-heat conversion performance, albeit no reports of functional WS<sub>2</sub> nanoparticles (NPs)/silk fibroin exhibiting photothermal conversion characteristics have been published to date. Because of the superior photothermal characteristics and nontoxicity of WS<sub>2</sub> nanoparticles, they have become a safer choice in the textile manufacturing industry [15,16]. One such use was shown by Yang et al. [17], who employed WS<sub>2</sub> nanosheets to construct a novel dressing fabric that was near-infrared photo-responsive. A combination of chitosan, WS<sub>2</sub> nanosheets, and ciprofloxacin was used to create this kind of novel material. The benefits of this nanocomposite dressing are that it has strong tissue adherence as well as great biocompatibility. Toxicological studies performed on human cells revealed that the aqueous 2D WS<sub>2</sub> suspension had no effect on cell survival and only a limited role in facilitating oxidative stress [18]. The wet spinning technique was utilized in prior work to create RSF fibers, which allowed the functioning nanoparticles to be mixed straightforwardly into the spinning solutions. This method was shown to be effective in both functionalizing RSF fibers and maintaining the tensile potency of RSF fibers [19–22]. With the aid of wet spinning, the present research has, for instance, created photochromic RSF/WO<sub>3</sub> NPs fiber exhibiting exceptional durability and photochromic capabilities under sunlight [23]. People, particularly those living in colder climates, are becoming more interested in spontaneous heating fabrics [24].

Using wet spinning, a sequence of RSF/WS<sub>2</sub> nanoparticles hybrid fibers having varying concentrations of WS<sub>2</sub> nanoparticles were created and tested in this study (Fig. 1). The simulated sunshine test revealed that the temperatures of hybrid fibers containing 0.8 wt% RSF/WS<sub>2</sub> nanoparticles might increase from 20.4°C to 85.6°C in one minute and 108.3°C in ten minutes when exposed to simulated sunlight. In addition, once the WS<sub>2</sub> nanoparticles are incorporated into the blend of fibers, the toughness has the potential to increase. The reason behind the improvement of mechanical characteristics of hybrid regenerated yarn was discussed through crystallinity, and smaller crystalline size of RSF/WS<sub>2</sub> nanoparticles hybrid fibers, as well as β-sheet content in the regenerated fibroin solution. By employing such RSF/WS<sub>2</sub> nanoparticle hybrid fibers, it is possible to create silk textile easily that has a spontaneous heating function when exposed to sunlight.

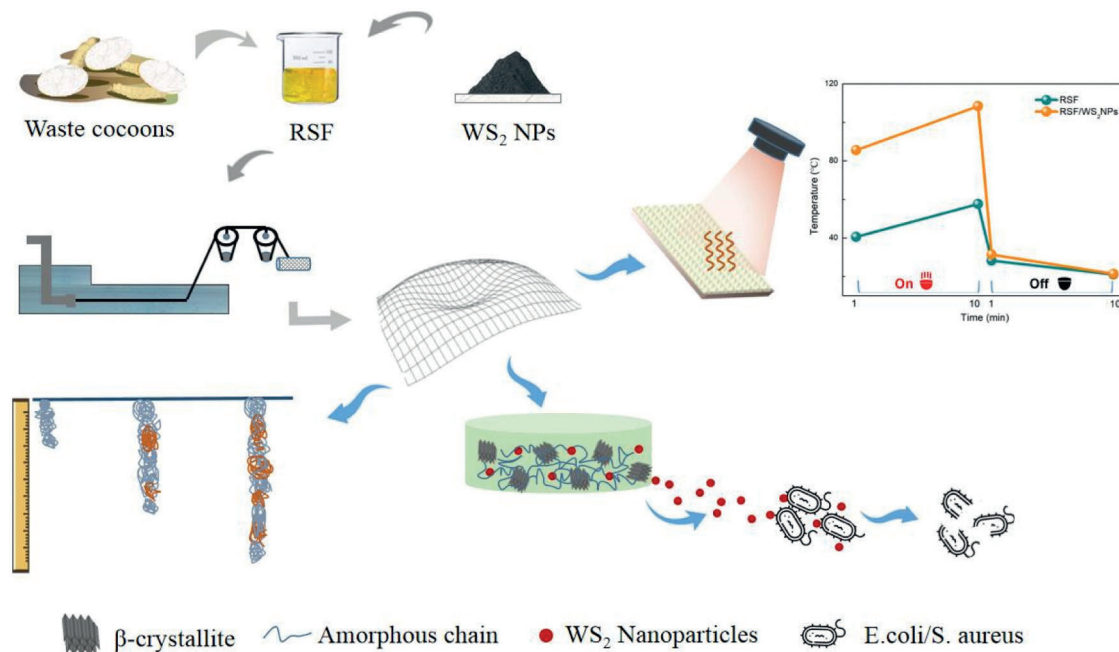


**Figure 1:** Schematic illustration of RSF/WS<sub>2</sub> NPs hybrid fibers with high toughness and photothermal properties

## 2 Materials and Methods

### 2.1 Materials

Waste cocoons derived from *Bombyx mori* silkworm (Chinese Academy of Agricultural Sciences, Zhenjiang, China), WS<sub>2</sub> nanoparticles (Jiangsu Xianfeng Nanomaterials Technology Co., Ltd., Nanjing, China), absolute ethanol (C<sub>2</sub>H<sub>5</sub>OH) (Sinopharm Group Chemical Reagent Co., Ltd., Beijing, China), sodium carbonate (Na<sub>2</sub>CO<sub>3</sub>) (Sinopharm Group Chemical Reagent Co., Ltd., Beijing, China), Formic acid (FA) (Shanghai Aladdin Co., Ltd., Shanghai, China), anhydrous calcium chloride (CaCl<sub>2</sub>) (Sinopharm Group Chemical Reagent Co., Ltd., Beijing, China).

### 2.2 Procedure for Preparing the Spinning Solution

A bath ratio of 1:20 was used to combine the silkworm cocoon shells with the 0.05 weight percent Na<sub>2</sub>CO<sub>3</sub> hydrated solution, followed by heating for 30 min and washing thrice using ultrapure water at 60°C to eliminate contaminants and residual ions from the cocoon shells. The silk degumming experiment described above was carried out thrice. Finally, the degummed silks were left to dry at 45 degrees Celsius for 3 days. In order to make a solution of regenerated silk fibroin, the degummed silk was dissolved in 5 weight percent CaCl<sub>2</sub>-FA solution for four hours at 24°C. Varying masses of WS<sub>2</sub> NPs were introduced to the silk fibroin solution and mixed continuously. We found that the weight ratios of WS<sub>2</sub> NPs to degummed silk were as follows: 0.04 weight percent, 0.2 weight percent, 0.4 weight percent, 0.8 weight percentage, 1.2 weight percentage, and 2.0 weight percentage.

### 2.3 Preparation of the Hybrid Fibers

In the present research, a handmade wet spinning apparatus was employed, and all trials were carried out at a temperature of 24°C. Subsequently, we eliminated air bubbles from the spinning solution through static positioning for 30 min after it had been put into a medical syringe. A high-pressure injection pump was utilized to compress the spinning solution vertically in the syringe into the coagulation bath at a

temperature of 24°C, which enabled the spinning solution to quickly condense into homogeneous fibers. Following the stretching procedure, the RSF fibers were immersed in a 75 percent ethanol solution for 2 h to eliminate any remaining solvent from the fibers' structure. Finally, we removed the RSF fibers and left them to dry at a temperature of 24°C.

#### 2.4 Procedure for Preparing Fluorescence Spectroscopy Test Samples

A 4 mL tube was filled with varying mass of WS<sub>2</sub> NPs, 3 mL silk fibroin solution with a concentration of 10 mg/mL, 80 μL 1 mM Thioflavin T (ThT), and various mass of WS<sub>2</sub> NPs. We found that the WS<sub>2</sub> NPs to silk fibroin mass ratios were as follows: 0.04 weight percent, 0.2 weight percent, 0.4 weight percent, 0.8 weight percentage, 1.2 weight percentage, and 2.0 weight percentage, sequentially. For each of the samples, the fluorescence spectra of the solution were determined after they had been cultured at 24°C for 2, 4, 6, 8, 10, 12, and 24 h, respectively [25].

#### 2.5 Antibacterial Assay

Using *Escherichia coli* (*E. coli*) and *Staphylococcus aureus* (*S. aureus*) as test organisms, the antibacterial characteristics of the RSF/WS<sub>2</sub> NPs hybrid fibers were determined. The spread plate technique was utilized to seed 100 μL of diluted bacterial culture (containing approximately 10<sup>6</sup> colony-forming units per milliliter) onto the solidified nutrient agar medium, followed by the careful placing of the sterilized hybrid fiber (trimmed to approximately 15 mm in length and 3.5 mg in mass) on the plate's surface to allow the bacteria to colonize. Imaging of the plates was done after they had been incubated for 12 h at 37 degrees Celsius, and the diameters of the blocks were quantified utilizing Image-J software to determine their size.

#### 2.6 Characterization

RSF/WS<sub>2</sub> NPs hybrid fibers were examined at 20 kV utilizing field emission scanning electron microscopy (JSM-IT500HR, Japan) after being coated with gold with the aid of a sputter coater to determine their morphological characteristics. Fourier transform infrared spectroscopy (FTIR, Nicolet iS10, USA) combined with diamond ATR accessories were utilized to examine the morphological alteration of RSF/WS<sub>2</sub> NPs hybrid fibers. The fibroin solution was subjected to a fluorescence test by means of the F-4600 (Hitachi, Japan). A 420-nm excitation wavelength and a 5-nm slit are used in the present research, and the range of the emission wavelength is 430–700 nm. In the present protocol, the photothermal characteristics of WS<sub>2</sub> NPs hybrid fibers were examined utilizing a xenon lamp (CEL-HXF300-T3, λ ≥ 420 nm, 300 W, China). Subsequently, the thermogravimetric analyzer (TGA) (Q5000, TA Instruments, USA) was employed to assess the thermal deterioration of silk fabrics. The heating of the silk fibroin samples was performed at a rate of ten degrees Celsius each minute to increase the temperature from ambient to 600°C in N<sub>2</sub>. We also recorded the derivative thermogravimetry (DTG) curves as well as the thermogravimetric (TG) curves.

With the aid of the mechanical test equipment (Instron 3343, USA) containing a 10 N load cell, mechanical testing was performed on a single fiber in both RSF fibers as well as RSF hybrid fibers at a relative humidity of 40 ± 5% and temperature of 24 ± 0.5 degrees Celsius. The gage length was determined to be 6 millimeters whereas the stretching rate was determined to be 2 millimeters per minute.

X-ray diffraction (Rigaku TTR-III, Japan) was used to examine the internal architectures of WS<sub>2</sub> NPs hybrid fibers. A copper target (CuKα, λ = 0.1542) was employed as a radiation source while 40 kV was the amount of voltage used in the experiment. The crystallinity (*Xc*) of fibers was obtained using an equation as follows:  $Xc = \frac{I_c}{I_c + I_a} \times 100$ . *I<sub>a</sub>* and *I<sub>c</sub>* denote the amorphous peak integral intensity and crystallization peak integral intensity. The Debye-Scherrer equation may be used to determine the size of

crystallites as illustrated below:  $L = \frac{0.9\lambda}{\beta \cos \theta}$ , where L denotes the grain size on the crystallographic planes,  $\lambda$  denotes the CuK $\alpha$  wavelength,  $\beta$  denotes the half peak width,  $\theta$  denotes the angular diameter of diffraction.

### 3 Results and Discussion

#### 3.1 Morphological Characteristics of WS<sub>2</sub> NPs and RSF Fibers

The SEM image (Fig. 2b) and TEM image (Fig. 2a) of the WS<sub>2</sub> NPs showed that the structure of the WS<sub>2</sub> NPs was comparable to a flake whose average dimension was 110 nm. As illustrated in Figs. 2c and 2d, the surfaces of 0.8 wt% RSF/WS<sub>2</sub> NPs hybrid fibers were shown to be smooth and homogeneous free of any cavities or fractures in the interior structure. We discovered that the fibers had an average diameter of  $37.82 \pm 1.15 \mu\text{m}$ . As the phenomena of agglomeration could not be observed on the SEM pictures of the RSF hybrid fibers, it is possible that the NPs exhibit a high degree of distribution in the hybrid fibers. As a result, adding nanoparticles to RSF fibers had no effect on their initial structure or qualities, and it was these traits that contributed to the excellent mechanical performance of RSF fibers.

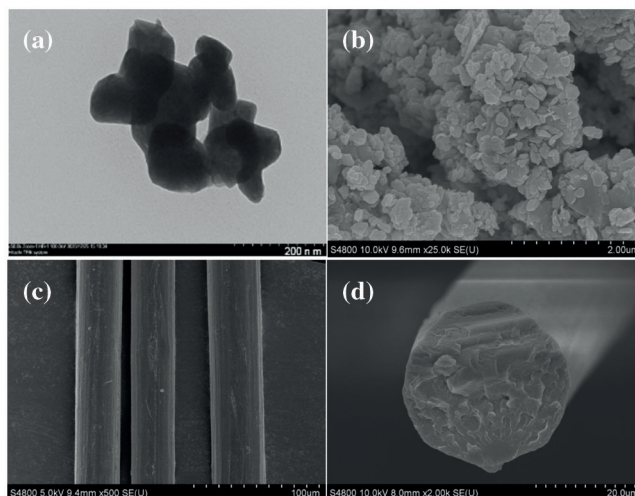


**Figure 2:** (a) TEM image of WS<sub>2</sub> nanoparticles; (b) SEM image of WS<sub>2</sub> nanoparticles. SEM images of 0.8 wt% RSF/WS<sub>2</sub> NPs hybrid fibers; (c) Surface structure; (d) Internal structure

Following thermal disintegration, the SEM-EDS component spectrum of the 0.8 weight percent RSF/WS<sub>2</sub> NPs hybrid fiber was shown in Fig. 3. A consistent dispersion of C, N, O, S, and W components in the hybrid fiber was observed, demonstrating that the WS<sub>2</sub> NPs were evenly dispersed throughout the fiber. Table 1 shows the proportion of each element present in the hybrid fiber and their relative proportions. C, N, O, S, and W made up 78.97%, 6.32%, 13.74%, 0.08%, and 0.89% of the total, respectively.

#### 3.2 Mechanical Characteristics of Hybrid Fibers Based on RSF/WS<sub>2</sub> NPs

Fig. 4 illustrates the elongation at the break-breaking strength curves for RSF fibers as well as RSF/WS<sub>2</sub> NPs hybrid fibers, demonstrating that the hybrid fibers exhibit significantly greater elasticity as opposed to the RSF fibers. Owing to the exceptional breaking elongation of hybrid fibers with 0.8 wt percent and 0.4 wt% WS<sub>2</sub> NPs, the fibers have a greater toughness. Table 2 indicates comprehensive data on the mechanical characteristics of the material. The hybrid fibers containing 0.8 weight percent WS<sub>2</sub> NPs displayed the most superior mechanical characteristics. In contrast with the RSF fibers, the breaking strength (264.59 MPa) and elongation-at-break (115.92%) of the 0.8 wt% WS<sub>2</sub> NPs hybrid fibers increase

to 1.69 and 2.71 times on average, respectively. For example, 6 mm hybrid fibers can be stretched to 13 mm. Furthermore, it was discovered that as the WS<sub>2</sub> NPs content increased, the average mechanical properties values of WS<sub>2</sub> NPs hybrid fibers rose first and descended later (Table 2), illustrating that too many WS<sub>2</sub> NPs lead to the deterioration of mechanical characteristics of fibers. According to these results, it was concluded that WS<sub>2</sub> nanoparticles exhibited a considerable toughening impact on RSF fibers.

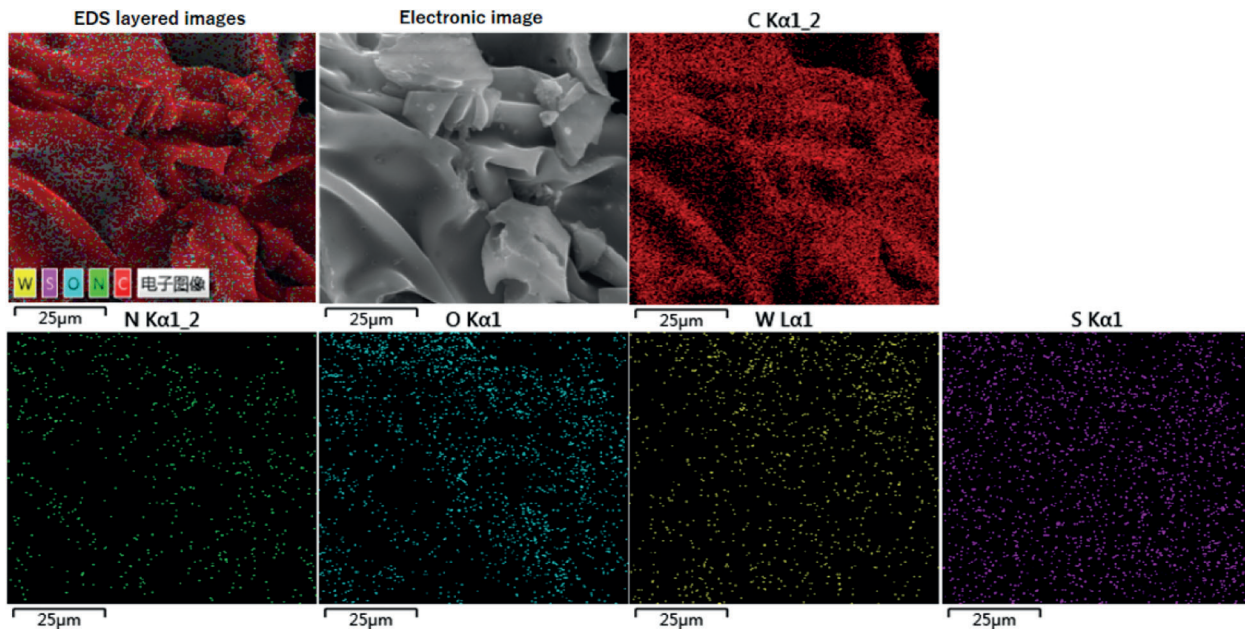


**Figure 3:** EDS images of 0.8 wt% RSF/WS<sub>2</sub> NPs hybrid fibers residues after thermal decomposition

**Table 1:** Elemental analysis of 0.8 wt% RSF/WS<sub>2</sub> NPs hybrid fibers residues after thermal decomposition

Elements	The relative percentage contents/%
C	78.97
N	6.32
O	13.74
S	0.08
W	0.89

### 3.3 Photothermal Properties of RSF/WS<sub>2</sub> NPs Hybrid Fabric and Fibers

Because the inclusion of WS<sub>2</sub> NPs in RSF fibers was shown to be beneficial to the mechanical characteristics of the fibers, additional explorations into their photothermal capabilities were carried out. In the present research, the temperature of the fiber's surface was measured after being exposed to radiation with a W xenon lamp ( $\lambda \geq 420$  nm) for 1, 3, 5, and 10 min, respectively, and cooled for 1, 3, 5, and 10 min following the removal of the source light were visualized utilizing an infrared imager (Fig. 5). In the case where the light was absent, no temperature change was observed between RSF fibers and hybrid fibers containing 0.8 wt% RSF/WS<sub>2</sub> NPs (Fig. 5b). Compared to pure RSF fibers, the temperatures of hybrid fibers containing 0.8 wt% RSF/WS<sub>2</sub> NPs rose dramatically quicker under

simulated illumination. RSF/WS<sub>2</sub> NPs hybrid fibers were shown to heat up from 20.4°C to 85.6°C in 1 min and reach 108.3°C in 10 min (Figs. 5c and 5d), whereas the RSF's temperatures were shown to only increase by a small amplitude from 40.5°C and 57.5°C at both of these two-time periods. Fig. 6 depicted the alterations in temperature of RSF/WS<sub>2</sub> NPs hybrid fibers as a function of time when heated and cooled. According to Fig. 6, the hybrid fibers' temperature increased more rapidly in contrast with that of the RSF fiber during the same irradiation duration, and its ultimate temperature was greater in a similar manner. When the source of light was switched off for ten minutes, the temperatures of the two fibers were restored to nearly the same level.

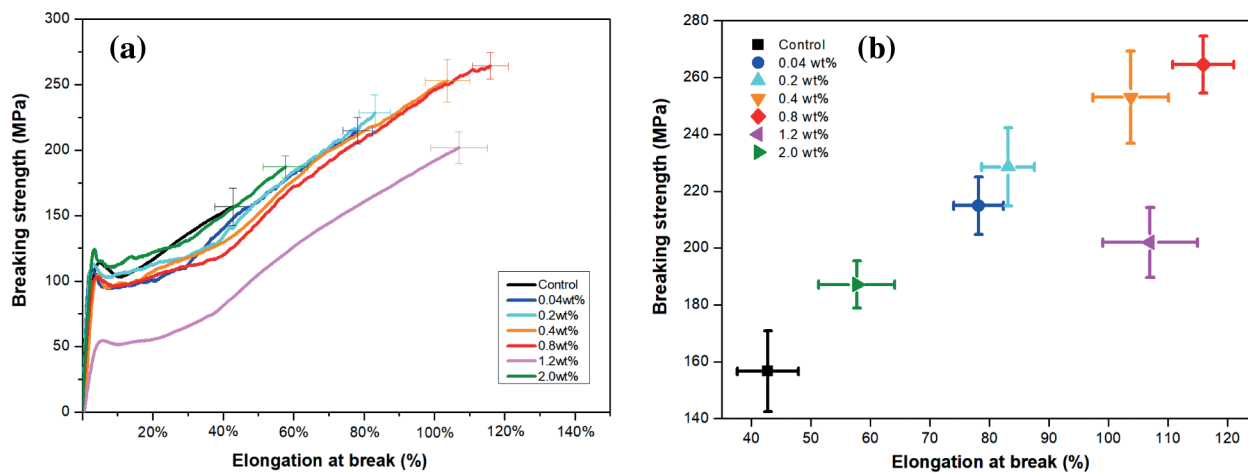


**Figure 4:** The elongation at break-breaking strength (a) curves (b) values of RSF/WS<sub>2</sub> NPs hybrid fibers with different WS<sub>2</sub> NPs contents

**Table 2:** The mechanical properties of RSF/WS<sub>2</sub> NPs hybrid fibers

Sample	Breaking strength/MPa	Elongation at break/%
Control	156.65 ± 14.29	42.75 ± 5.11
RSF/WS <sub>2</sub> NPs-0.04 wt%	214.92 ± 10.12	78.17 ± 4.15
RSF/WS <sub>2</sub> NPs-0.2 wt%	228.54 ± 13.85	83.11 ± 4.46
RSF/WS <sub>2</sub> NPs-0.4 wt%	253.04 ± 16.23	103.74 ± 6.36
RSF/WS <sub>2</sub> NPs-0.8 wt%	264.59 ± 10.03	115.92 ± 5.15
RSF/WS <sub>2</sub> NPs-1.2 wt%	201.97 ± 12.25	107.01 ± 7.98
RSF/WS <sub>2</sub> NPs-2.0 wt%	187.19 ± 8.26	57.69 ± 6.42

The ultimate objective of this research was to create a spontaneously heat-generating silk fabric that could be used in everyday life. The 0.8 weight percent RSF/WS<sub>2</sub> NPs hybrid fibers were manually woven into the fabric in order to evaluate the spontaneously heating capability of the RSF/WS<sub>2</sub> NPs-based material. The temperature of the fabric's surface was measured utilizing infrared imaging, which was similar to the approach used to evaluate the fibers aforementioned. In only 10 min of irradiation, the temperature of the area produced of RSF/WS<sub>2</sub> NPs hybrid fiber rose from 32.7°C to 116.8°C (Fig. 7c), whereas the temperature of the part created of RSF fiber alone increased to 84.2°C after the same time period. When they were allowed to cool for 10 min, their temperatures dropped to 37.4°C and 36.3°C, correspondingly (Fig. 7e). As a consequence, it was concluded that even a very tiny quantity of WS<sub>2</sub> NPs

had a considerable photothermal impact in the RSF/WS<sub>2</sub> NPs hybrid fibers. Based on these findings, we hypothesized that the RSF/WS<sub>2</sub> NP hybrid fibers have a wide range of potential applications in the production of RSF textiles with spontaneous heating functions in the presence of sunlight.

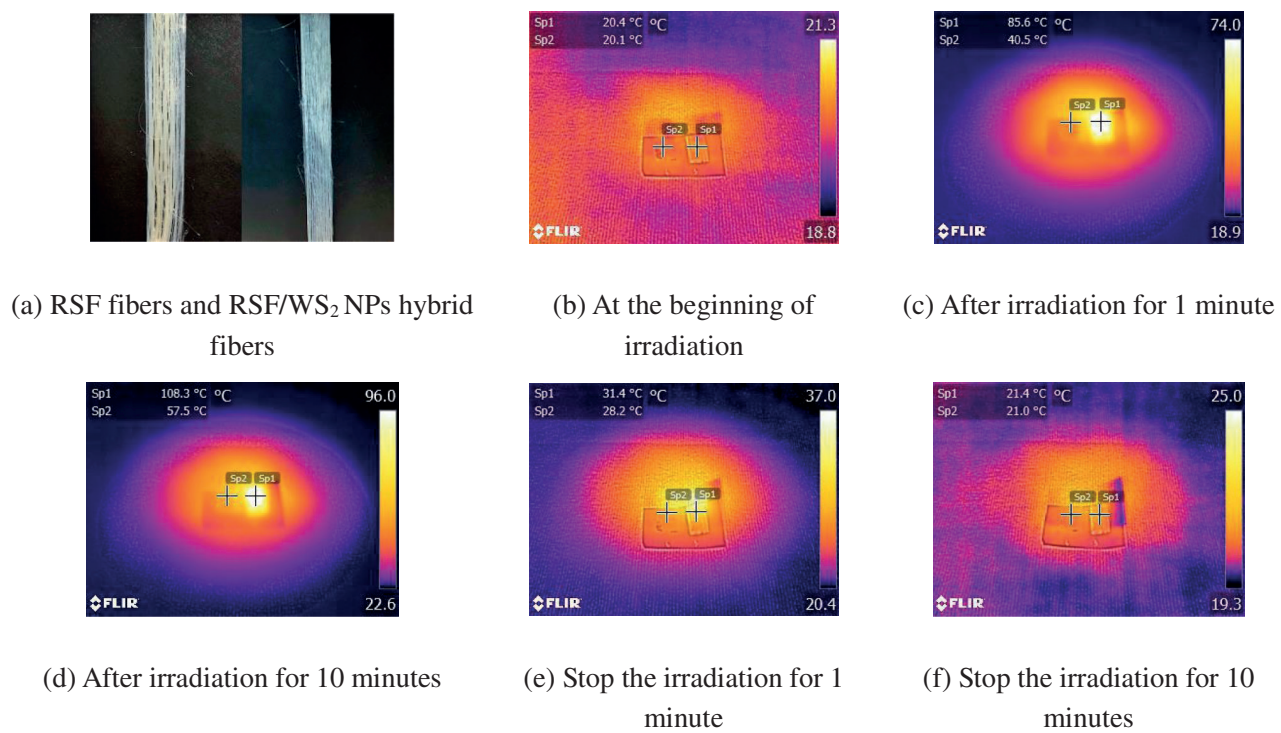


**Figure 5:** Temperature change of RSF fibers and 0.8 wt% RSF/WS<sub>2</sub> NPs hybrid fibers under the irradiation of simulated sunlight

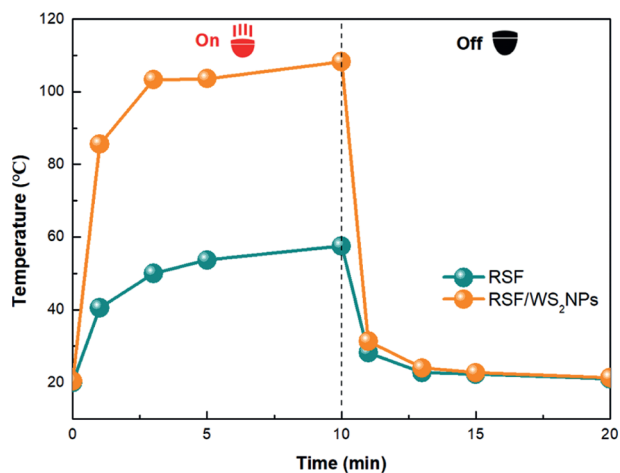


**Figure 6:** The temperature changes of RSF fibers and 0.8 wt% RSF/WS<sub>2</sub> NPs hybrid fibers during heating and cooling

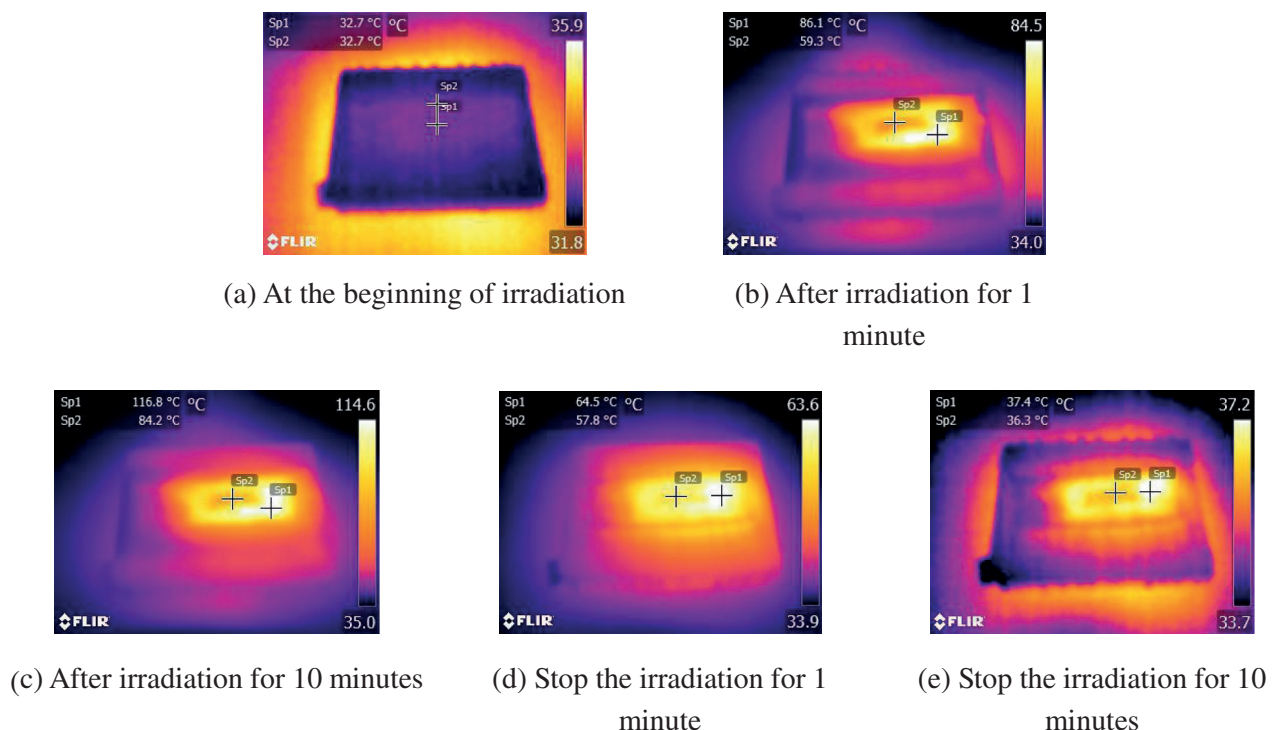


**Figure 7:** Temperature change of RSF/WS<sub>2</sub> NPs woven fabric under the irradiation of simulated sunlight

The ability to use human radiation and the self-heating performance of the fabric on the human body is another advantage of fabric application. The temperature change of RSF/WS<sub>2</sub> NPs fabric under natural sunlight from 11 am to 12 am (local time) on sunny winter days in Zhenjiang, China, was used to evaluate the self-heating performance of RSF/WS<sub>2</sub> NPs fabric, which is a critical factor in smart warm clothing. Then RSF/WS<sub>2</sub> NPs fabric and RSF fabric were respectively worn on the left and right wrists of volunteer to investigate the actual photothermal property (Fig. 8c). After natural sunlight irradiation for 10 min, the temperature of the hand wearing RSF/WS<sub>2</sub> NPs fabric reached 38.3°C (Fig. 8a), which was higher than the temperature of the hand wearing RSF fabric (26.4°C) and surrounding air (12.0°C). Infrared thermal imaging test results showed that the temperature of RSF/WS<sub>2</sub> NPs fabric reached 40.2°C, and demonstrated excellent self-heating effect (Fig. 8e). The excellent self-heating performance of RSF/WS<sub>2</sub> NPs fabric can be attributed to many aspects. For example, the photothermal conversion performance of two-dimensional WS<sub>2</sub> NPs, WS<sub>2</sub> NPs uniformly distributed in the fabric can improve the absorption area and reflection pathway of human radiation (Fig. 8b).

### 3.4 Thermal Stability of RSF/WS<sub>2</sub> NPs Hybrid Fibers

RSF fibers, as well as 0.8 weight percent RSF/WS<sub>2</sub> NPs hybrid fibers, were subjected to TGA to determine their thermal stability. As illustrated in Fig. 9, hybrid fibers with RSF/WS<sub>2</sub> NPs and single-mode fibers with RSF are both represented by their first-order differential curve (DTG) and TG curves. According to the findings, RSF, and 0.8 wt% RSF/WS<sub>2</sub> NPs hybrid fibers exhibited a similar thermal reaction mechanism showing a two-step weight drop for both fiber types. Fig. 9a depicts the dehydration phase as the first step, which occurred at a temperature ranging from 25 to 120 degrees Celsius. The second phase was the thermal deterioration stage, which occurred at a temperature of around 260°C. At 600°C, the weight-loss rates of 0.8 wt% RSF/WS<sub>2</sub> NPs hybrid fibers were almost the same as those of the RSF fibers, which were 63.86% and 64.28%, respectively (Fig. 9a). According to Fig. 9b, the

maximum thermal deterioration rate of RSF fibers and RSF/WS<sub>2</sub> NPs hybrid fibers appeared at about 297.1°C. It demonstrated that the addition of WS<sub>2</sub> NPs only had little effect on the thermal decomposition process of RSF fibers and maintained the thermal stability of the RSF fibers.

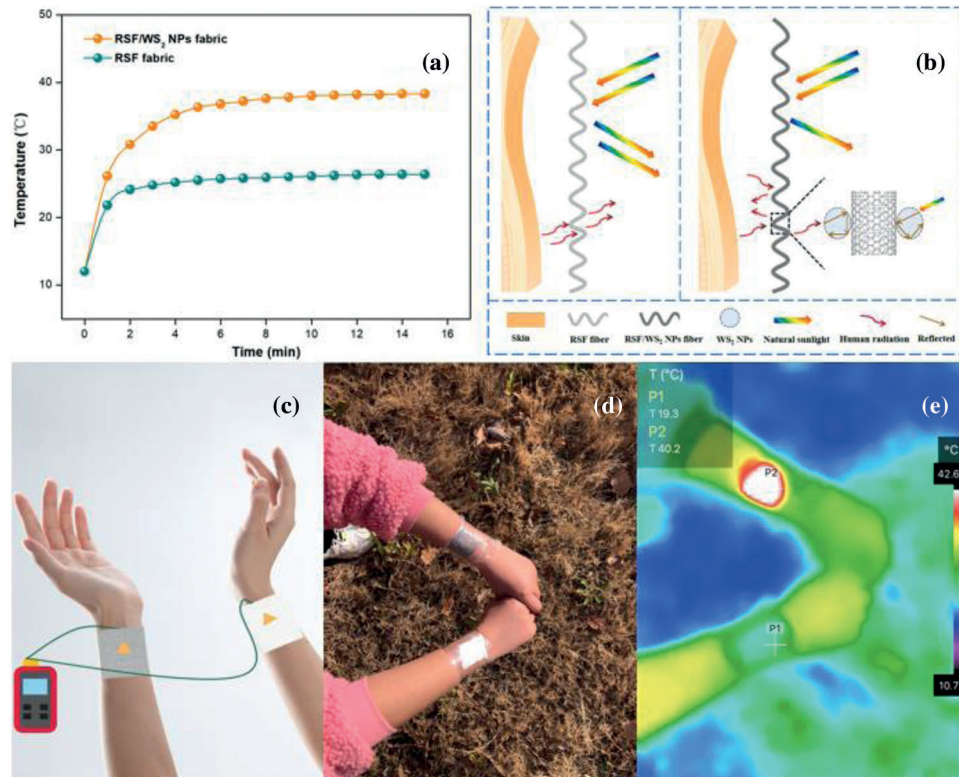


**Figure 8:** (a) Temperature change of the wrist under natural light; (b) Diagram of the photothermal conversion process with RSF/WS<sub>2</sub> NPs fabric and RSF fabric; (c) Schematic of testing wrist temperature; (d, e) IR image of fabrics for warming a volunteer' wrist under natural sunlight for 15 min

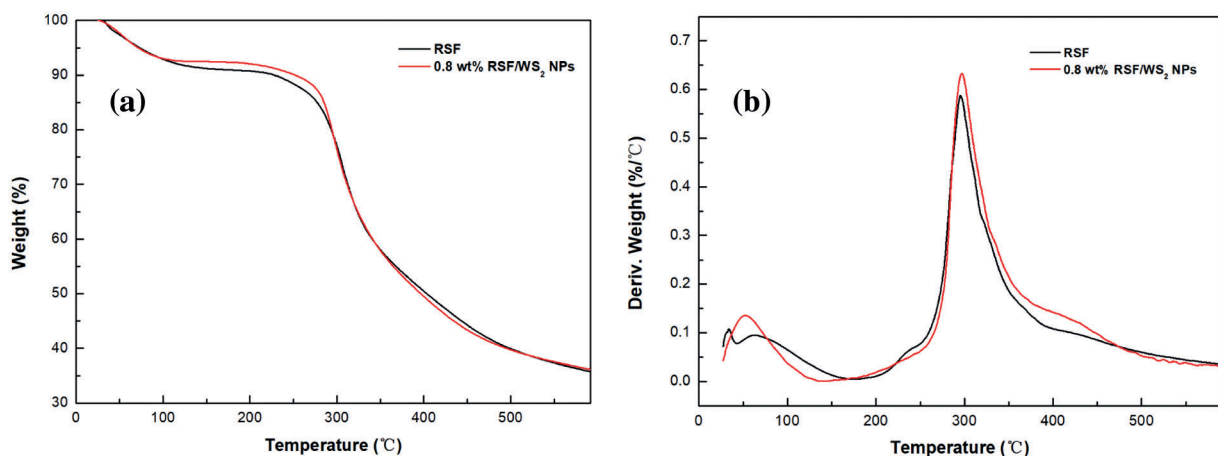


**Figure 9:** (a) TG curves of RSF/WS<sub>2</sub> NPs hybrid fibers and RSF fibers; (b) DTG curves of RSF/WS<sub>2</sub> NPs hybrid fibers and RSF fibers

### 3.5 FT-IR Analysis of RSF/WS<sub>2</sub> NPs Hybrid Fibers

Moreover, we discovered that the secondary structures of silks were strongly associated with their mechanical qualities (such as toughness modulus, elongation at break, and breakage strength) [26]. The superior interior structure of the silks was investigated utilizing FTIR, a feasible method for the purpose of evaluating the secondary morphology of silks [27]. For example, as illustrated in Fig. 10a, both RSF fibers and RSF/WS<sub>2</sub> NPs hybrid fibers exhibit peak locations that are almost identical in their corresponding FTIR spectra, demonstrating that WS<sub>2</sub> NPs have no impact on the secondary structural components of RSF fibers.

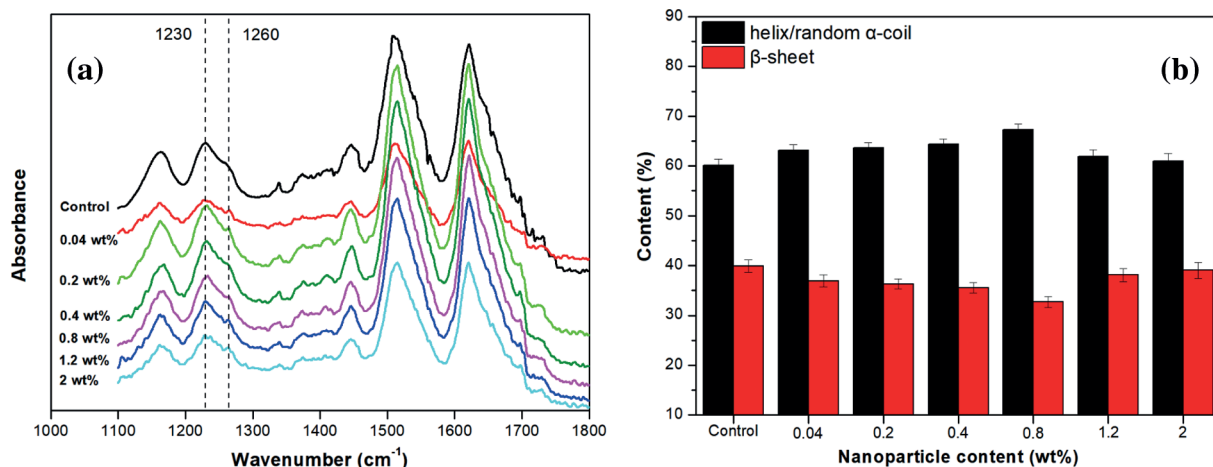


**Figure 10:** (a) FTIR patterns of RSF fibers and RSF/WS<sub>2</sub> NPs hybrid fibers; (b) The secondary structures contents of RSF/WS<sub>2</sub> NPs hybrid fibers with different WS<sub>2</sub> NPs contents

We de-convoluted the amide III spectral area of both the RSF fibers and RSF/WS<sub>2</sub> NPs hybrid fibers for the purpose of probing into what was in the secondary structural components of both materials [28]. Fig. 10b depicted the concentration of  $\beta$ -sheet ( $1260\text{ cm}^{-1}$ ) and  $\alpha$ -helix/random coil ( $1230\text{ cm}^{-1}$ ) in RSF and RSF/WS<sub>2</sub> NPs hybrid fibers. As opposed to RSF fibers, the helix and random coil of the RSF/WS<sub>2</sub> NPs hybrid fibers are greatly increased, while the  $\beta$ -sheet is less. When the concentration of nanoparticles present in the RSF/WS<sub>2</sub> hybrid fiber was 0.8 weight percent and the concentration of  $\beta$ -sheet was at its lowest level. These results indicated that the integration of WS<sub>2</sub> NPs suppressed or blocked the transition from  $\alpha$ -helix/random coil of RSF fibers to  $\beta$ -sheet, or that this integration was not favorable to the creation of  $\beta$ -sheet.

In the process of mixing and twirling the spinning liquid solution containing WS<sub>2</sub> NPs, the interplay between silk fibroin and the nanoparticle surfaces might ultimately cause reorganization of silk fibroin molecules and alter silk fibroin agglomeration. Moreover, the nanoparticles binding to silk fibroin altered the equilibria constants of  $\beta$ -sheet development, which slowed down the creation of both the crucial nucleus and the  $\beta$ -sheet [29]. In the case where the concentration of WS<sub>2</sub> NPs in RSF was greater than 0.8 weight percent, we assumed they would form small-scale agglomerations, which would prevent all nanoparticles from completely contacting the silk fibroin. WS<sub>2</sub> nanoparticles will grow in size after being aggregated, indicating that the incorporation of WS<sub>2</sub> nanoparticles had little impact on the ability to self-assemble of silk fibroin. Even now, providing a coherent elucidation for the changing trend in the composition of secondary structure is a difficult task.

### 3.6 XRD Analysis of RSF/WS<sub>2</sub> NPs Hybrid Fibers

The technique of X-ray diffraction (XRD) is commonly utilized to delve into the crystalline structure of RSF fibers [30–32]. The location and strength of diffraction peaks in RSF fibers may serve as a tool to

determine the crystalline structure of the fibers. Fig. 11a depicts the XRD patterns of RSF fibers and hybrid fibers containing 0.8 weight percent RSF/WS<sub>2</sub> NPs. The mechanical qualities of 0.8 weight percent RSF/WS<sub>2</sub> NPs hybrid fibers were found to be the best, Hence, the XRD pattern of these fibers was chosen for the purpose of performing a comparison to the RSF fibers. RSF fibers and hybrid fibers containing 0.8 weight percent of RSF/WS<sub>2</sub> NPs showed no statistically significant change in their XRD patterns. For example, as illustrated in Figs. 11b and 11d, the a, b, and c orientations are represented by three crystal planes, namely (200), (210), and (002). In the present research, the peak fitting approach was used to estimate the crystalline nature and average  $\beta$ -sheet crystal sizes, followed by calculation using the equation [33,34]. RSF/WS<sub>2</sub> NPs hybrid fibers were investigated for their crystal size and crystalline structure, as indicated in Table 3. The crystallinity, as well as crystal size of RSF/WS<sub>2</sub> NPs hybrid fibers, were found to be lower compared to those of RSF fibers. In view of their large specific surface area and abundance of active sites on the surface [35], WS<sub>2</sub> NPs might strongly interface with the fibroin matrix via  $\pi$ - $\pi$  stacking, electrostatic, hydrogen bonding, van der Waals, or hydrophobic interplay, which might also prevent the helix and random coils from morphing into  $\beta$ -sheets, resulting in the reduction of the  $\beta$ -sheets [36,37]. A reduction in the transformation of  $\beta$ -sheets to crystalline phase was a result of these findings. For this reason, adding WS<sub>2</sub> nanoparticles to silk fibroin ended up causing the crystallization of RSF/WS<sub>2</sub> nanoparticles hybrid fibers to substantially reduce, which is in agreement with the findings of the FTIR experiment. Increased phase boundaries might be generated by crystal refining, which would result in greater plastic deformation impedance for the RSF/WS<sub>2</sub> NPs hybrid fibers, as well as increased hardness for the fibers.

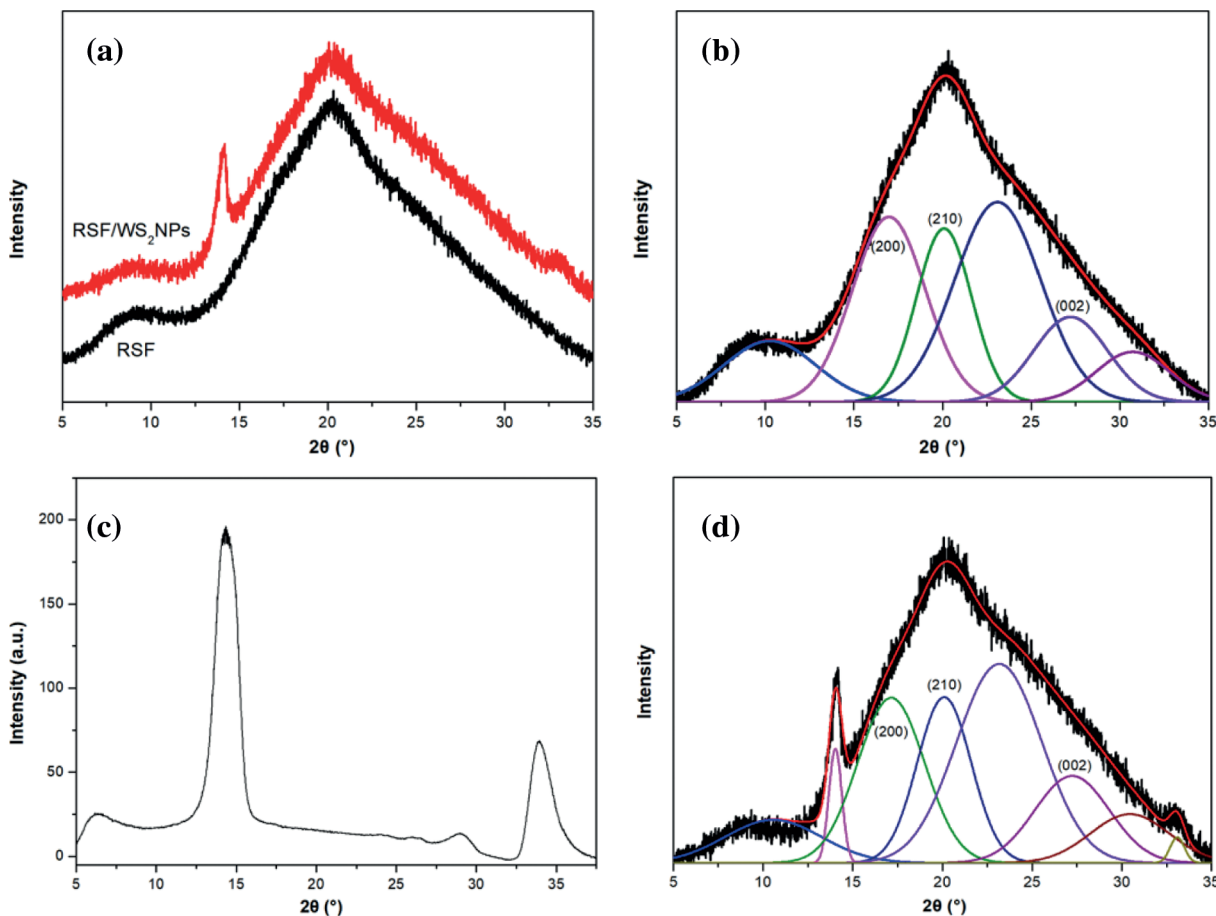


**Figure 11:** (a) XRD pattern of RSF fibers and 0.8 wt% RSF/WS<sub>2</sub> NPs hybrid fibers; (b) XRD pattern deconvolution of RSF fibers; (c) XRD of WS<sub>2</sub> NPs; (d) XRD pattern deconvolution of 0.8 wt% RSF/WS<sub>2</sub> NPs hybrid fibers

**Table 3:** Structural parameters of RSF fibers and 0.8 wt% RSF/WS<sub>2</sub> NPs hybrid fibers

Sample	Crystallinity/%	L <sub>hkl</sub> /nm			V/nm <sup>3</sup>
		(200)	(210)	(002)	
Control	41.25	2.35	1.68	1.59	6.28
RSF/WS <sub>2</sub> NPs-0.8 wt%	37.48	1.82	1.27	1.66	3.84

Nova et al. [26] demonstrated that the final toughness of spider silk was regulated by the toughness of  $\beta$ -sheets nanocrystals and this strength was strongly correlated with the size of these  $\beta$ -sheets nanocrystals. A fiber's toughness is determined by the number of crystals inside it. Keten et al. [38] also considered that the size of the crystallites seemed to have a significant impact on the mechanical characteristics of the fibers. Under lesser stresses, the bigger crystallite of the fibers was being disintegrated. However, the tiny crystallites may possess the capacity to withstand distortion and breakage under higher forces. The cracking of RSF fibers undergoing fracturing might well be deflected by nanoparticles with a modest size impact, which could increase the toughness of RSF fibers [39,40]. As a result, we hypothesized that WS<sub>2</sub> NPs prevented the production of bigger  $\beta$ -sheets crystals in the fiber, which could lead to an increase in uniformly distributed crystals and an improvement in toughness in the final product. Once the composition of WS<sub>2</sub> NPs in the RSF/WS<sub>2</sub> NPs hybrid fibers reached over 0.8 weight percent, the mechanical characteristics of the hybrid fibers started to deteriorate, which might be caused by the unevenly distributed excess WS<sub>2</sub> NPs concentration inside the hybrid fibers.

### 3.7 Effect of WS<sub>2</sub> NPs on the Self-Assembly Behavior of RSF in Solution

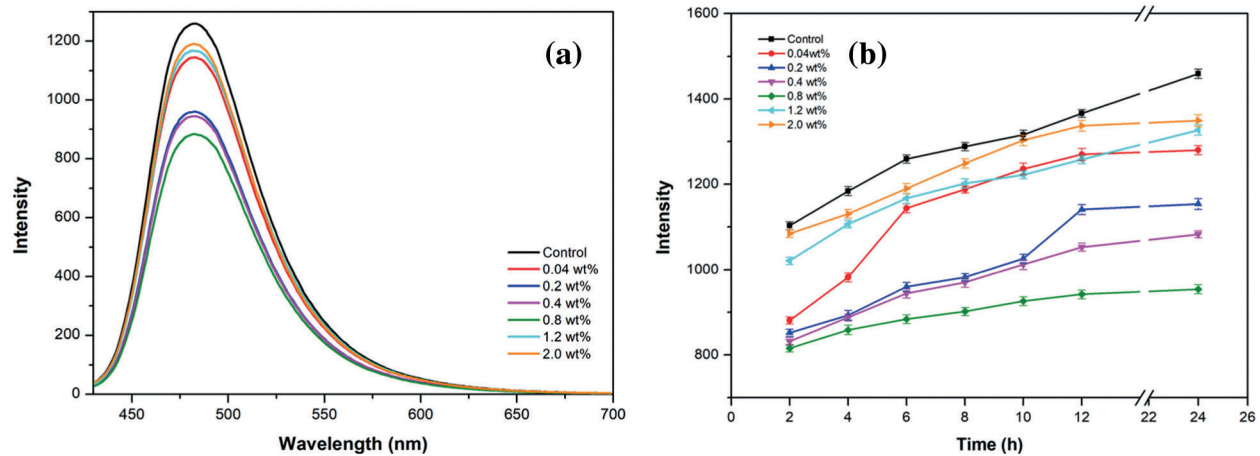
Thioflavin T (ThT) is recognized as a fluorescent dye that could attach to the  $\beta$ -sheet in proteins with high specificity [41]. Because the intensity of the fluorescence is equivalent to the amount of  $\beta$ -sheet present in the system, the ThT fluorescent probe may have the ability to determine the concentration of  $\beta$ -sheet present in the system [42]. Fig. 12a depicted the fluorescence spectrum of varying weight fractions of WS<sub>2</sub> NPs mixed with RSF solution for 6 h. It has been shown that the lesser the fluorescence value, the lesser the  $\beta$ -sheet concentration, and the weaker  $\beta$ -sheet self-assembly in RSF solution. When RSF alone was added to the solution, greater fluorescence intensity was observed. When the amount of WS<sub>2</sub> NPs used was below 0.8 weight percent, the proportion of  $\beta$ -sheet in the RSF solution reduced as a result of adding WS<sub>2</sub> NPs to the solution. The lowest fluorescence intensity was observed when the WS<sub>2</sub> NPs concentration was 0.8 weight percent, indicating that the solution contained the lowest amount of  $\beta$ -sheet. Overall, these findings were in line with the results of the FT-IR test of the RSF/WS<sub>2</sub> NPs hybrid fiber conducted before.

Fig. 12b depicted the fluctuation in fluorescence intensity of RSF/WS<sub>2</sub> NPs solution over time and at various weight fractions in the whole process of the experiment. According to Fig. 12b, at each point tested, the fluorescence intensity of the 0.8 weight percent RSF/WS<sub>2</sub> NPs solution was the smallest. These findings indicated that WS<sub>2</sub> NPs inhibited the formation of a  $\beta$ -sheet in RSF solution in a dosage-dependent way.

### 3.8 Antibacterial Activity Against *E. Coli* and *S. Aureus* in Vitro

The bacterial growth-inhibition halos of the RSF/WS<sub>2</sub> NPs hybrid fibers were measured to determine their antibacterial properties. Bacteria grown on various fibers incubated for 12 h were shown in Fig. 13. Antibacterial action in the RSF fibers is nonexistent; microorganisms flourished unhindered around the fibers (Figs. 13a and 13c). Nevertheless, the suppression zones were clearly observed surrounding the RSF/WS<sub>2</sub> NPs hybrid fibers, and when these zones were measured in terms of sizes against *E. coli* (*S.*

*aureus*), they were found to be 1.2 mm (1.5 mm) (Figs. 13b and 13d). Obviously, the RSF/WS<sub>2</sub> NPs hybrid fibers had certain antibacterial action against *S. aureus* and *E. coli*. Research has previously indicated that the antibacterial action of the RSF/WS<sub>2</sub> NPs hybrid fibers against *S. aureus* and *E. coli* was directly related to the oxidase-like activity of WS<sub>2</sub> NPs [43]. Probably, the use of WS<sub>2</sub> NPs contributes to higher antibacterial action against *S. aureus* in contrast with a gram-negative bacterium. Our findings demonstrated that the integration with WS<sub>2</sub> NPs could impart certain antibacterial properties to the hybrid fibers.



**Figure 12:** (a) The fluorescence emission spectra of RSF/WS<sub>2</sub> NPs solution with different mass fractions at 6 h. (b) The fluorescence intensity of RSF/WS<sub>2</sub> NPs solution with different mass fractions changed with time

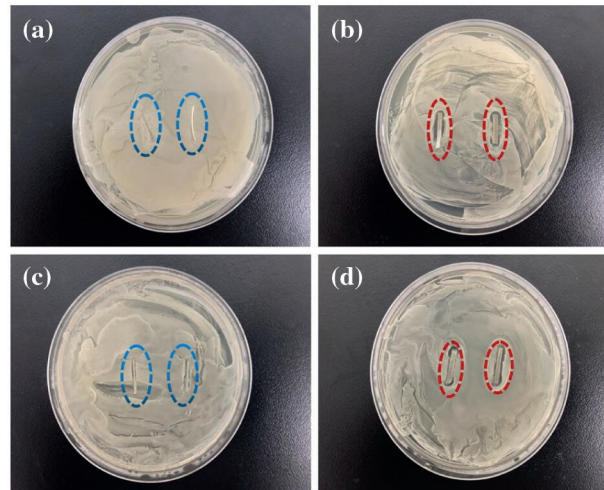


**Figure 13:** Antibacterial activities of 0.8 wt% RSF/WS<sub>2</sub> NPs hybrid fibers. Images of nutrient broth agar covered by *E. coli* with fibers (a) RSF fibers; (b) 0.8 wt% RSF/WS<sub>2</sub> NPs hybrid fibers. Images of nutrient broth agar covered by *S. aureus* with fibers (c) RSF fibers; (d) 0.8 wt% RSF/WS<sub>2</sub> NPs hybrid fibers

#### 4 Conclusions

In summary, RSF/WS<sub>2</sub> NPs hybrid fibers with greater tenacity, antibacterial activity, and photothermal characteristics were prepared through the wet spinning technique. Also revealed was that the inclusion of

WS<sub>2</sub> NPs decreased the β-sheet concentration, crystalline nature, as well as crystal size in the hybrid fibers, which could contribute to the increased tenacity of RSF/WS<sub>2</sub> NPs hybrid fibers. The Thioflavin T fluorescence spectrum test was also utilized to validate the decrease in the β-sheet concentration in the silk fibroin solution. In the case where the WS<sub>2</sub> NPs composition was 0.8 weight percent, the mechanical characteristics of the produced hybrid fibers were shown to be the best they could be. Moreover, the photothermal properties of both the hybrid fibers and the knitted fabric were found to be excellent. Therefore, it is concluded that the information provided in the present research on WS<sub>2</sub> NPs augmented RSF will be useful in the design as well as fabrication of more novel functional fibers in the future. Overall, the present research provides a method for manufacturing fibers with excellent toughness and photothermal capabilities that can be used in multifunctional fibers.

**Date Availability:** The raw data required to reproduce these findings can be obtained upon request to ghwu@just.edu.cn.

**Funding Statement:** This research was funded by the Education Department of Guizhou Provincial Project (No. KY2016277, China), the Science and Technology Department of Guizhou Provincial Project (No. LH20157693, China), the Jiangsu Specially Appointed Professor Program (No. Sujiaoshi201517, China), the National Project of Risk Assessment for Quality and Safety of Special Agro-Products (No. GPFP201701003, China).

**Conflicts of Interest:** The authors declare that they have no conflicts of interest to report regarding the present study.

## References

1. Shirvanimoghaddam, K., Motamed, B., Ramakrishna, S., Naebe, M. (2020). Death by waste: Fashion and textile circular economy case. *Science of the Total Environment*, 718, 137317. DOI 10.1016/j.scitotenv.2020.137317.
2. Stanesco, M. D. (2021). State of the art of post-consumer textile waste upcycling to reach the zero waste milestone. *Environmental Science and Pollution Research*, 28(12), 14253–14270. DOI 10.1007/s00500-021-05935-7.
3. Kasavan, S., Yusoff, S., Guan, N. C., Zaman, N. S. K., Fakri, M. F. R. (2021). Global trends of textile waste research from 2005 to 2020 using bibliometric analysis. *Environmental Science and Pollution Research*, 28(33), 44780–44794. DOI 10.1016/j.ijar.2019.06.009.
4. Seib, F. P. (2021). Emerging silk material trends: Repurposing, phase separation and solution based designs. *Materials*, 14(5), 1160. DOI 10.1016/S0898-1221(19)00056-5.
5. Deng, T. T., Cheng, L., Peng, Y. W., Tong, X. L., Guo, N. K. et al. (2019). Structure and properties of bombyx mandarina silk fiber and hybrid silk fiber. *Journal of Natural Fibers*, 18(3), 330–342. DOI 10.1080/15440478.2019.1623743.
6. Tao, H., Kaplan, D. L., Omenetto, F. G. (2012). Silk materials: A road to sustainable high technology. *Advanced Materials*, 24(21), 2824–2837. DOI 10.1002/adma.201104477.
7. Vepari, C., Kaplan, D. L. (2007). Silk as a biomaterial. *Progress in Polymer Science*, 32(8), 991–1007. DOI 10.1016/j.progpolymsci.2007.05.013.
8. Pan, H., Zhang, Y. P., Shao, H. L., Hu, X. C., Li, X. H. et al. (2014). Nanoconfined crystallites toughen artificial silk. *Journal of Materials Chemistry B*, 2(10), 1408–1414. DOI 10.3934/mbe.2020321.
9. Hu, X. J., Li, J. G., Bai, Y. X. (2017). Fabrication of high strength graphene/regenerated silk fibroin composite fibers by wet spinning. *Materials Letters*, 194, 224–226. DOI 10.1016/j.knosys.2012.11.012.
10. Zhou, X. F., Sun, H. N., Bai, X. (2020). Two-dimensional transition metal dichalcogenides: Synthesis, biomedical applications and biosafety evaluation. *Frontiers Bioengineering and Biotechnology*, 8, 236. DOI 10.32604/cmc.2022.019345.

11. Kumar, P., Roy, S., Sarkar, A., Jaiswal, A. (2021). Reusable MoS<sub>2</sub> modified antibacterial fabrics with photothermal disinfection properties for repurposing of personal protective masks. *ACS Applied Materials Interfaces*, *13*(11), 12912–12927. DOI 10.1021/acsami.1c00083.
12. Cao, F. Y., Wei, C. M., Ma, G. Q., Hou, L. K., Zhang, R. C. et al. (2021). Synthesis of photothermal antimicrobial cotton gauze using AuNPs as photothermal transduction agents. *RSC Advances*, *11*(42), 25976–25982. DOI 10.1109/ACCESS.2021.3118055.
13. Hong, J., Park, C., Kim, Y. (2019). Photothermal properties of wool fabrics colored with SiO<sub>2</sub>@ AuNPs. *Colloids and Surfaces A*, *574*, 115–121. DOI 10.31181/dmame180101P.
14. Nie, X. L., Wu, S. L., Huang, F. L., Wang, Q. Q., Wei, Q. F. (2021). Smart textiles with self-disinfection and photothermochromic effects. *ACS Applied Materials Interfaces*, *13*(2), 2245–2255. DOI 10.1016/j.asoc.2018.01.012.
15. Yi, H. Y., Zhou, X. Y., Zhou, C. H., Yang, Q. Y., Jia, N. Q. (2021). Liquid exfoliated biocompatible WS<sub>2</sub>@BSA nanosheets with enhanced theranostic capacity. *Biomaterials Science*, *9*(1), 148–156. DOI 10.1016/S0898-1221(03)00016-6.
16. Zhang, T., Ma, T., Li, W. P. (2015). Preparation of ultrahigh molecular weight polyethylene/WS<sub>2</sub> composites for bulletproof materials and study on their bulletproof mechanism. *Journal of Macromolecular Science, Part B: Physics*, *54*(8), 992–1000. DOI 10.1080/00222348.2015.1035689.
17. Yang, N., Zhu, M., Xu, G. C., Liu, N., Yu, C. (2020). A near infrared light responsive multifunctional nanocomposite hydrogel for efficient and synergistic antibacterial wound therapy and healing promotion. *Journal of Materials Chemistry B*, *8*(17), 3908–3917. DOI 10.1016/j.ins.2010.11.004.
18. Domi, B., Bhorkar, K., Rumbo, C., Sygellou, L., Martin, S. M. et al. (2021). Toxicological assessment of commercial monolayer tungsten disulfide nanomaterials aqueous suspensions using human A549 cells and the model fungus *Saccharomyces cerevisiae*. *Chemosphere*, *272*, 129603. DOI 10.1007/BF01001956.
19. Zhang, W. W., Zhang, D. S., Chen, Y. Y., Lin, H. (2015). Hyperbranched polymer functional TiO<sub>2</sub> nanoparticles: Synthesis and its application for the anti-UV finishing of silk fabric. *Fibers and Polymers*, *16*(3), 503–509. DOI 10.1016/j.asoc.2011.01.003.
20. Wang, H. P., Dong, Q. L., Yao, J. R., Shao, Z. Z., Ma, J. M. et al. (2020). Colorless silk/copper sulfide hybrid fiber and fabric with spontaneous heating property under sunlight. *Biomacromolecules*, *21*(4), 1596–1603. DOI 10.1021/acs.biomac.0c00170.
21. Liu, Y., Wang, X. L., Xu, C., Ma, Q., Wu, G. H. (2020). Effect of nano titanium dioxide on mechanical properties of regenerated silk. *IOP Conference Series: Materials Science and Engineering*, *892*, 012006. DOI 10.1088/1757-899X/892/1/012006.
22. Guo, J. J., Yang, B., Ma, Q., Fometu, S. S., Wu, G. H. (2021). Photothermal regenerated fibers with enhanced toughness: Silk fibroin/MoS<sub>2</sub> nanoparticles. *Polymers*, *13*, 3937. DOI 10.3390/polym13223937.
23. Ma, Q., Yang, B., Li, H. H., Guo, J. J., Zhao, S. Q. et al. (2021). Preparation and properties of photochromic regenerated silk fibroin/tungsten trioxide nanoparticles hybrid fibers. *Composites Communications*, *27*, 2452–2139. DOI 10.1016/j.coco.2021.100810.
24. Wang, F., Gao, C., Kuklane, K., Holmer, I. (2010). A review of technology of personal heating garments. *International Journal of Occupational Safety and Ergonomics*, *16*(3), 387–404. DOI 10.1080/10803548.2010.11076854.
25. Konar, S., Sen, S., Pathak, A. (2017). Morphological effects of CuO nanostructures on fibrillation of human serum albumin. *Journal of Physical Chemistry B*, *121*(51), 11437–11448. DOI 10.1021/acs.jpcb.7b08432.
26. Nova, A., Keten, S., Pugno, N. M., Redaelli, A., Buehler, M. J. (2010). Molecular and nanostructural mechanisms of deformation, strength and toughness of spider silk fibrils. *Nano Letters*, *10*(7), 2626–2634. DOI 10.1021/nl101341w.
27. Ling, S. J., Qi, Z. M., Knight, D. P., Shao, Z. Z., Chen, X. (2011). Synchrotron FTIR microspectroscopy of single natural silk fibers. *Biomacromolecules*, *12*(9), 3344–3349. DOI 10.1021/bm2006032.
28. Lin, N. B., Cao, L. W., Huang, Q. L., Wang, C. Y., Wang, Y. et al. (2016). Functionalization of silk fibroin materials at mesoscale. *Advanced Functional Materials*, *26*(48), 8885–8902. DOI 10.1002/adfm.201603826.

29. Shemetov, A. A., Nabiev, I., Sukhanova, A. (2012). Molecular interaction of proteins and peptides with nanoparticles. *ACS Nano*, 6(6), 4585–4602. DOI 10.1021/nn300415x.
30. Fang, G. Q., Zheng, Z. K., Yao, J. R., Chen, M., Tang, Y. Z. et al. (2015). Tough protein/carbon nanotube hybrid fibers comparable to natural spider silks. *Journal of Materials Chemistry B*, 3(19), 3940–3947. DOI 10.1039/c5tb00448a.
31. Peng, Q. F., Shao, H. L., Hu, X. C., Zhang, Y. P. (2015). Role of humidity on the structures and properties of regenerated silk fibers. *Progress in Natural Science: Materials International*, 25(5), 430–436. DOI 10.1016/j.pnsc.2015.09.006.
32. Zhang, X. N., Gong, D. C., Gong, Y. X. (2019). Insight into the orientation behavior of thermal-aged and historic silk fabrics by polarized FTIR microspectroscopy. *Journal Cultural Heritage*, 38, 53–63. DOI 10.1016/j.culher.2019.02.007.
33. Fu, S. Y., Wei, C. C., Yang, J. M., Chen, T. H. (2016). Crystallite size variations of nanosized Fe<sub>2</sub>O<sub>3</sub> powders during γ-to α-phase transformation. *Nano Letters*, 2, 245–252. DOI 10.1021/nl010089m.
34. Zhang, H. C., Bhunia, K., Munoz, N., Li, L., Dolgovskij, M. et al. (2017). Linking morphology changes to barrier properties of polymeric packaging for microwave assisted thermal sterilized food. *Journal of Applied Polymer Science*, 134(44), 45481. DOI 10.1002/app.45481.
35. Liu, W. W., Feng, Y. Q., Yan, X. B., Chen, J. T., Xue, Q. J. (2013). Superior micro supercapacitors based on graphene quantum dots. *Advanced Functional Materials*, 23(33), 4111–4122. DOI 10.1002/adfm.201203771.
36. Li, L., Wu, G. H., Yang, G. H., Peng, J., Zhao, J. W. et al. (2013). Focusing on luminescent graphene quantum dots: Current status and future perspectives. *Nanoscale*, 5(10), 4015–4039. DOI 10.1039/c3nr33849e.
37. Ling, S. J., Li, C. X., Adamcik, J., Wang, S. H., Shao, Z. Z. et al. (2014). Directed growth of silk nanofibrils on graphene and their hybrid nanocomposites. *ACS Macro Letters*, 3(2), 146–152. DOI 10.1021/mz400639y.
38. Keten, S., Xu, Z. P., Ihle, B., Buehler, M. J. (2010). Nanoconfinement controls stiffness, strength and mechanical toughness of beta-sheet crystals in silk. *Nature Materials*, 9(4), 359–367. DOI 10.1038/NMAT2704.
39. Fu, S. Y., Feng, X. Q., Lauke, B., Mai, Y. W. (2008). Effects of particle size, particle/matrix interface adhesion and particle loading on mechanical properties of particulate polymer composites. *Composites Part B*, 39(6), 933–961. DOI 10.1016/j.compositesb.2008.01.002.
40. Lauke, B., Fu, S. Y. (2013). Aspects of fracture toughness modelling of particle filled polymer composite. *Composites Part B*, 45(1), 1569–1574. DOI 10.1016/j.compositesb.2012.07.021.
41. Wu, C., Biancalana, M., Koide, S., Shea, J. E. (2009). Binding modes of Thioflavin-T to the single layer β-sheet of the peptide self-assembly mimics. *Journal of Molecular Biology*, 394(4), 627–633. DOI 10.1016/j.jmb.2009.09.056.
42. Wang, J. N., Yi, H. G., Wei, Y. Q. (2011). Preliminary biocompatibility evaluation of regenerated antheraea yamamai silk fibroin *in vitro*. *Journal of Wuhan University of Technology Materials Science Edition*, 26(6), 1044–1048. DOI 10.1007/s11595-011-0360-8.
43. Liu, X., Duan, G. X., Li, W. F., Zhou, Z. F., Zhou, R. H. (2017). Membrane destruction mediated antibacterial activity of tungsten disulfide (WS<sub>2</sub>). *RSC Advances*, 7(60), 37873–37880. DOI 10.1039/c7ra06442j.